Author(s): Tarvainen, Olli; Kalvas, Taneli; Toivanen, Ville; Kosonen, Sami; Koivisto, Hannu; Hill, Clive; Bainbridge, Alex; Hinton, Alex; Shepherd, Ben; Faircloth, Dan

Title: Ion source and low energy beam transport prototyping for a single-ended heavy ion ToF-ERDA facility

Year: 2023

Version: Published version

Nuclear Instruments and Methods in Physics Research B 538 (2023) 110–114

Contents lists available at ScienceDirect

Nuclear Inst. and Methods in Physics Research, B

journal homepage: www.elsevier.com/locate/nimb

Ion source and low energy beam transport prototyping for a single-ended heavy ion ToF-ERDA facility

Olli Tarvainen [a,*], Taneli Kalvas [b], Ville Toivanen [b], Sami Kosonen [b], Hannu Koivisto [b], Clive Hill [c], Alex Bainbridge [d], Alex Hinton [d], Ben Shepherd [d], Dan Faircloth [a]

[a] UK Research and Innovation, Science and Technology Facilities Council, Rutherford Appleton Laboratory, ISIS Neutron and Muon Source, Harwell, OX110QX, UK
[b] Accelerator Laboratory, Department of Physics, University of Jyväskylä, Jyväskylä, FI-40014, Finland
[c] UK Research and Innovation, Science and Technology Facilities Council, Daresbury Laboratory, Technology Department, Warrington, WA44AD, UK
[d] UK Research and Innovation, Science and Technology Facilities Council, Daresbury Laboratory, ASTeC, Warrington, WA44AD, UK

ARTICLE INFO

Keywords:
Time-of-flight elastic recoil detection analysis
Electron cyclotron resonance ion source
Low energy beam transport

ABSTRACT

We present the status of the ion source and low energy beam transport prototyping activities for a heavy ion time-of-flight elastic recoil detection analysis (ToF-ERDA) equipment, designed to accelerate a flux of 1–10 particle nano-Ampere of $^{40}Ar^{6-12+}$ ions to 3–6 MeV energy for depth profiling of light elements. The prototype injector consists of a novel permanent magnet electron cyclotron resonance ion source CUBE-ECRIS with a minimum-B quadrupole field topology, and a 90° permanent magnet dipole with adjustable field strength for charge state selection. We report experimentally measured argon beam currents as a function of the applied microwave power and ion source potential to demonstrate the feasibility of the CUBE-ECRIS as an injector for a single-ended ToF-ERDA facility with the ion source and low energy beam transport on a 500 kV platform without SF_6 electrical insulation. Finally, we present the design and field measurement results of the dipole magnet prototype.

1. Introduction

Time-of-Flight Elastic Recoil Detection Analysis (ToF-ERDA) facilities typically rely on negative ion sources and large tandem accelerators to achieve the relevant ion energies. The feasibility of low-energy ERDA and the implications of <10 MeV beam energies on the detector telescope design have been first discussed in Refs. [1,2]. Julin et al. have recently proposed a compact, large solid angle low energy ERDA spectrometer design, supported by Monte Carlo simulations and proof-of-concept experiments, suitable for incident beams with masses of 35–40 amu (e.g. ^{40}Ar) at 3–6 MeV energies [3]. The proposed design alleviates the accelerator requirements, which makes light element ToF-ERDA accessible for larger user base.

We report ion source and low energy beam transport activities aiming at the realisation of the single-ended ToF-ERDA facility utilising the above detector design. The concept shown schematically in Fig. 1 is based on a novel high charge state ECR ion source, CUBE-ECRIS [4], and a low energy beam transport with electrostatic focusing elements coupled with an adjustable field permanent magnet m/q-separator, on an air-insulated 500 kV platform. The benefits over the negative ion source — tandem accelerator scheme (also shown schematically in Fig. 1) are: increased reliability of the ion source, reduced operational effort and maintenance, lack of SF_6 electrical insulation and smaller laboratory footprint in comparison to most tandem-type accelerators.

The prototyping activities have been carried out to support the planning of the UK National Thin Film Deposition and Characterisation Centre (led by Daresbury Laboratory) and to scope an extension of the materials characterisation capabilities at ISIS Neutron and Muon Source (at Rutherford Appleton Laboratory). The proposed concept is intended to complement the arsenal of quantitative characterisation methods available for users by allowing the measurement of elemental depth profiles of thin films containing light elements, most importantly hydrogen and deuterium.

2. CUBE-ECRIS

The main benefit of the novel permanent magnet CUBE-ECR ion source, shown in Fig. 2, is the simplified magnet configuration requiring less permanent magnet material (NdFeB-N45H) in comparison to conventional >10 GHz ECR ion sources. The physics design and first results, e.g. argon charge state distributions, obtained with the ion source have been reported elsewhere [5] with the data available in

* Corresponding author.
E-mail address: olli.tarvainen@stfc.ac.uk (O. Tarvainen).

https://doi.org/10.1016/j.nimb.2023.02.035
Received 12 October 2022; Received in revised form 27 January 2023; Accepted 24 February 2023
Available online 7 March 2023

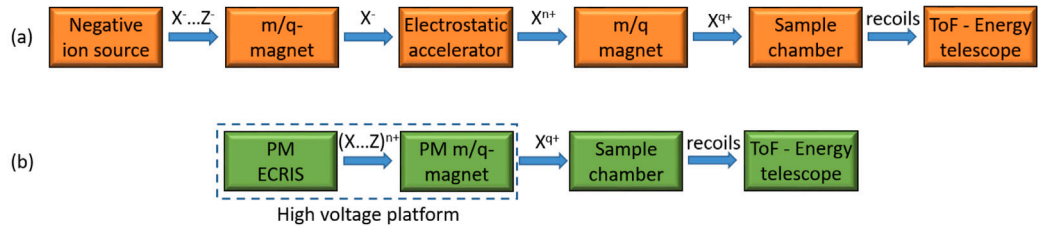

Fig. 1. Comparison of the ToF-ERDA concepts based on (a) negative ion source and tandem-type accelerator and (b) single-ended accelerator with a high charge state positive ion source on a high voltage platform.

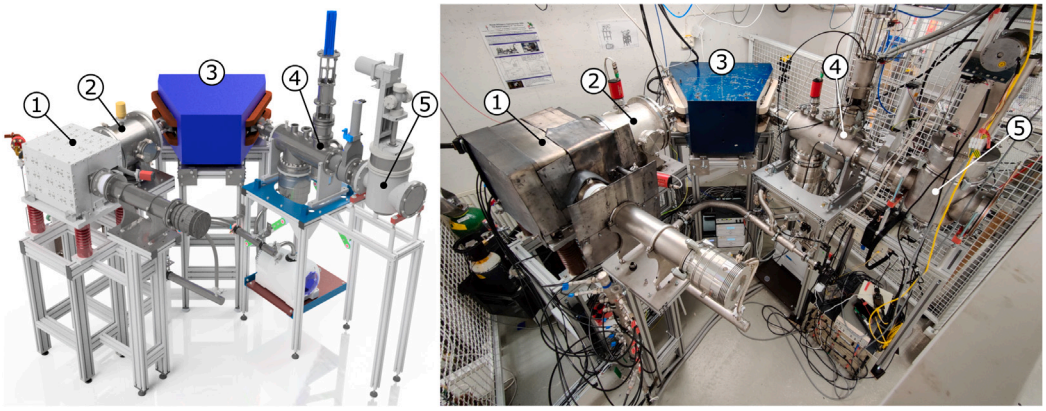

Fig. 2. A 3D model (left) and a photo (right) of the CUBE-ECRIS test stand. The main components of the system include the CUBE-ECRIS ion source (1), a quadrupole doublet for beam focusing (2), a 102° spectrometer magnet for m/q separation of ion beams (3), a Faraday cup for beam current measurements (4) and an Allison-type emittance scanner for beam quality studies (5).

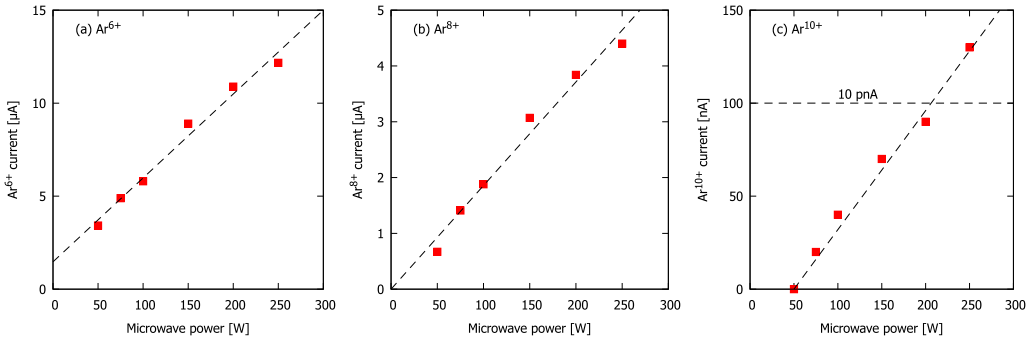

Fig. 3. The currents of (a) $^{40}Ar^{6+}$, (b) $^{40}Ar^{8+}$ and (c) $^{40}Ar^{10+}$ ion beams, extracted from the CUBE-ECRIS (8 mm round extraction aperture) as a function of the applied microwave power at 10.47 GHz with 10 kV source potential. The 10 pnA upper limit of IBA-relevant particle flux is marked in (c) with a dashed line.

open access repository [6]. Figs. 3 and 4 show the beam currents or argon charge states 6+, 8+ and 10+ as a function of the microwave power (10 kV source potential) and source potential (250 W microwave power) demonstrate that 1–10 pnA (particle nano-Ampere) ion fluxes, relevant for the IBA-application, have been produced already in the first experimental campaign, using an 8 mm diameter round extraction aperture. A smaller beam spot size in the scattering plane is desirable for the IBA-application, which needs to be taken into account in the design of the accelerating column and high energy beamline. One possibility to limit the beam size is to use collimator slits, which motivates further increase of the high charge state ion beam intensities from the ion source to maintain the desired flux at the target.

3. Permanent magnet dipole prototype

3.1. Physics design of the magnet

The physics design of the adjustable field permanent magnet dipole for heavy ion m/q-separation was carried out with Radia3D software [7]. The design took inspiration from the ZEPTO dipole magnet [8], developed at Daresbury Laboratory for the electron decelerator of the proposed Compact Linear Collider (CLIC). The heavy ion dipole magnet consists of (i) magnetic steel (AISI 1006) pole pieces, (ii) 4 mm thick permanent magnet (Neorem 712a, minimum B_r of 1.29 T), sandwiched between the pole pieces and (iii) magnetic steel return yoke

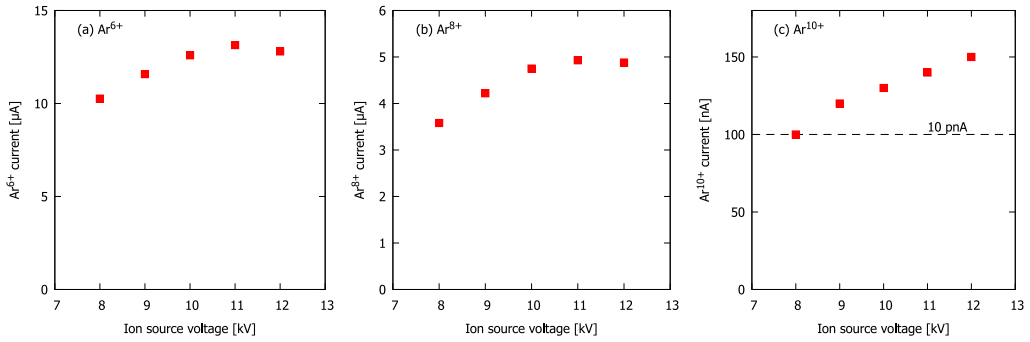

Fig. 4. The currents of (a) $^{40}Ar^{6+}$, (b) $^{40}Ar^{8+}$ and (c) $^{40}Ar^{10+}$ ion beams, extracted from the CUBE-ECRIS (8 mm round extraction aperture) as a function of the ion source potential with 250 W microwave power. The 10 pnA upper limit of IBA-relevant particle flux is marked in (c) with a dashed line.

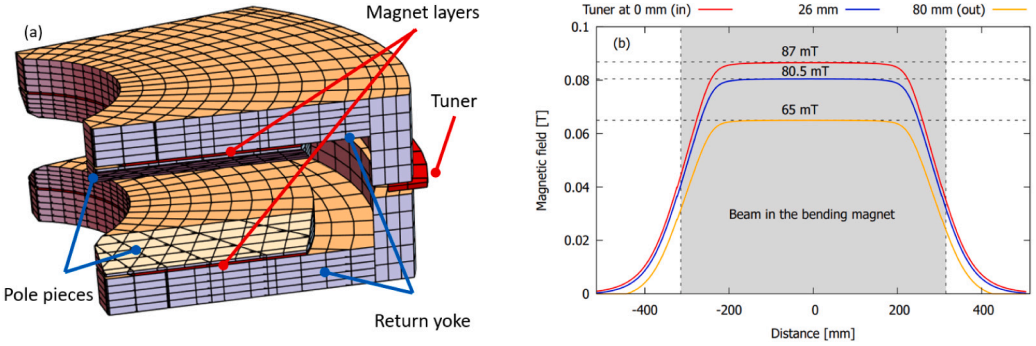

Fig. 5. (a) The Radia3D model of the permanent magnet dipole with the main parts identified. (b) The simulated magnetic field along the reference particle (beam) trajectory with three tuner magnet positions.

split in two halves with a 20 mm vertical gap reserved for (iv) an 8.4 mm thick permanent magnet "tuner cartridge" moving in the horizontal direction to adjust the magnetic field in the pole gap. The tuner is made of 12 permanent magnet (Neorem 712a) wedges. Fig. 5(a) shows the computational model of the magnet with the main parts labelled. The main parameters of the magnet are: 90° bending angle with a radius of 400 mm, pole gap of 90 mm, radial width of the pole pieces 300 mm, entrance angle of 35° and pole face shim angle of 30°. The linear stroke of the tuner cartridge motion is 80 mm; at 0 mm (fully in) the tuner magnets align radially with the 60 mm thick return yoke and at 80 mm (fully out) they are well outside the return yoke where their flux makes only a small contribution to the field in the pole gap. The simulated magnetic field along the reference trajectory is plotted in Fig. 5(b) for three tuner magnet positions demonstrating the field adjustment range and the "nominal design field" with the tuner at 26 mm. The field uniformity $\frac{\Delta B}{B}$ radially across the pole is expected to be better than 10^{-3} in 80 mm wide area around the optical axis (centre of the beam). This field uniformity requirement necessitates splitting the permanent magnet structure in three layers (pole layers and tuner). The magnetic field simulation for the physics design was done assuming the permanent magnet material to have a remanence field of 1.295 T, i.e. the minimum of the chosen magnet grade, to account for the worst case scenario. Thus, we expect the field to be up to 2.7% stronger in reality with nominal B_r of 1.33 T.

The range of the (design) magnetic fields allows transporting ^{40}Ar charge states from 6+ to 12+, relevant for the IBA application, through the dipole magnet by adjusting either the tuner position (magnetic field) at constant ion source potential or the ion source potential in the range of 8–13 kV. This is illustrated in Fig. 6 showing the required magnetic field as a function of the ion source potential and the simulated tuning range of the dipole magnet prototype. In the IBA-application the final energy of the beam is defined by the platform voltage and the ion charge state, which implies that the source potential is a free parameter for selecting the beam transported through the magnet.

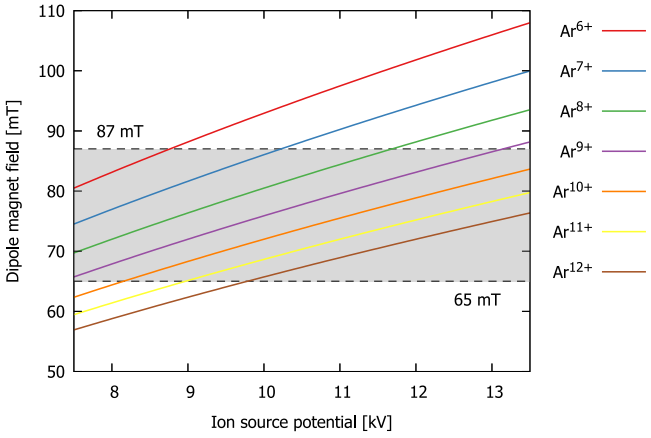

Fig. 6. The required magnetic field for argon charge states from 6+ to 12+ as a function of the ion source potential. The tuning range of the dipole magnet is indicated with the grey box.

Moreover, since the ion source potential can be adjusted to optimise the beam transport through the magnet, thermal management (magnetic shunt material or active cooling) is not required to compensate for the temperature-dependence of the permanent magnet remanence. Instead, this will be achieved with a feedback loop fine-tuning the ion source potential based on Hall-probe signal measuring the magnetic field in the pole gap. We note that maintaining a constant beam energy at the target requires adjusting the platform voltage accordingly. The energy resolution is defined by the (rms-)ripple of the platform high voltage power supply, which is typically better than 0.03% (as given by the manufacturer), i.e. 150 V for 500 kV platform voltage.

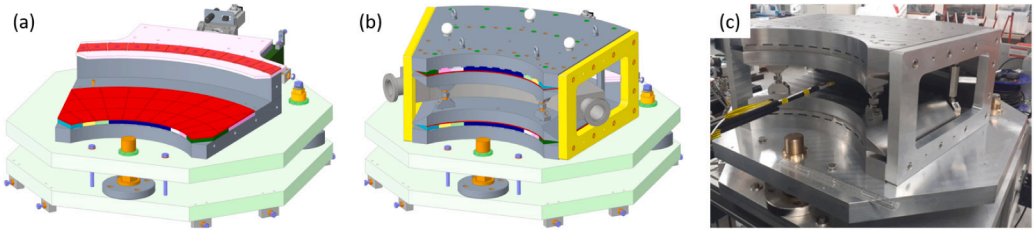

Fig. 7. The mechanical model of the permanent magnet dipole prototype. (a) The bottom half pole magnets and the tuner magnets are made visible. (b) The complete assembly model of the magnet with the vacuum chamber included. (c) A photograph of the magnet in the field measurement rig with the Hall probe reaching into the pole gap from left.

3.2. Mechanical design of the magnet

The mechanical design of the magnet and its assembly tooling was carried out by STFC's Technology Department at Daresbury Laboratory. The design is illustrated in Fig. 7. The thin permanent magnet layer, made visible in Fig. 7(a) is made out of 11 magnetic steel sector plates with the permanent magnet material glued on them. The magnetised sector plates are installed (and bolted to the return yoke) using bespoke assembly tooling enabling to manage the attractive force between each sector and the steel yoke. The tuner magnets form a "mosaic pattern" and are glued into recesses and clamped between two aluminium plates. The assembly is mirrored about the vertical midplane so that the final magnet assembly consists of two mechanically identical halves (as shown in Fig. 7(b)) with the magnetisation vector of the permanent magnet layers adjacent to the pole pieces pointing upwards. The magnetisation of the tuner magnets is in the opposite direction, thus completing the loop of the magnetic flux along the C-shaped yoke. The tuner cartridge is moved in/out with a linear drive. A photograph of the assembled magnet in the field measurement rig is shown in Fig. 7(c).

4. Magnetic field measurements

Measurements of the magnet were conducted in the magnet test laboratory at STFC Daresbury Laboratory, UK. All field measurements were taken using a Senis 3MH6 teslameter equipped with a Senis Type-C 3-axis Hall probe. This probe has a 30 × 30 μm active area in the vertical field direction and a 150 × 150 μm area in the transverse and longitudinal directions. This system is factory calibrated and manufacturer rated to better than 0.01% accuracy, and automatically corrects for planar Hall effect errors. The measurement area is climate controlled to $< \pm 1$ °C, and the probe features a temperature sensor with automatic compensation.

The probe was mounted on a rigid aluminium arm attached to a computer-controlled 3-axis motion system. The motion system uses absolute encoders with a repeatability error of <2 μm in the transverse and vertical directions and <5 μm in the longitudinal direction. The angle of rotation between the probe and the magnet axis is currently set manually and cannot be guaranteed better than 2°. The magnet was surveyed into position using laser tracking of the alignment fiducials relative to the motion system so that the magnet axes and motion system axes are well aligned. At each measurement point motion was paused, corrected onto the encoder, and 1000 flux density readings were taken from the probe at a 2 kHz sample rate whilst stationary. The mean reading of the flux density in each probe axis is recorded, along with the standard deviation and probe tip temperature.

Three types of measurements were carried out to benchmark the simulations against the measured field.

1. The vertical component of the magnetic field was measured at the midplane of the pole gap at the centre of the magnet pole piece as a function of the tuner position.
2. The vertical component of the magnetic field was measured moving the probe radially ±90 mm measured from the centre point.
3. The magnetic field components were measured in the vertical mid-plane of the magnet in a 2D grid of 180 × 344 mm with 2 mm step scanning from the fringe field of the magnet into the flat field region of the pole gap with different tuner positions.

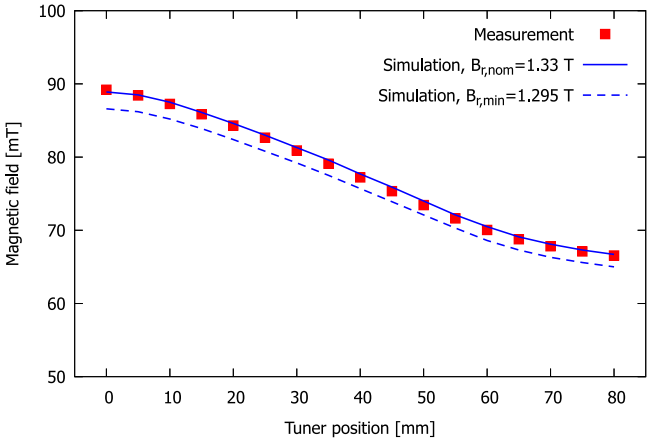

Fig. 8. The measured and simulated magnetic field in the pole gap centre point as a function of the tuner position (0 mm is fully in). The simulation was done for two permanent magnet remanence values — minimum and nominal.

This last measurement was done in order to model the beam transport in the entrance and exit of the magnet at a later stage, so the data are not plotted here.

Fig. 8 shows the measurement and simulation of the magnetic field (vertical component) in the pole gap at the centre of the pole. The simulation was done with two permanent magnet remanence values; assuming the minimum remanence of 1.295 T (worst case scenario) and the nominal remanence of 1.33 T as per the magnet data sheet [9]. The simulation with the nominal remanence matches with the measured field with an accuracy better than 0.5 mT across the whole movement range of the tuner whereas the (worst case) simulation with the minimum remanence produces 2–3% weaker field as expected. In conclusion the measurement validates the magnet design and the field adjustment range as designed.

The field data obtained in the radial scan at various tuner positions is presented and compared to the simulation (with B_r of 1.33 T) in Fig. 9(a). Here the division of the magnetic steel in Radia3D was optimised to produce the correct field profile with sufficient accuracy in the volume occupied by the beam in reasonable CPU time. The measured uniformity of the field in the ±40 mm radial width around the optical axis is shown in Fig. 9(b). Two conclusions can be drawn; the measured field matches the simulation and the uniformity of the field across the pole satisfies the specification of $\frac{\Delta B}{B} < 10^{-3}$ (radially) in the region relevant for beam transport regardless of the tuner position. In fact, the uniformity is better in the experiment than in the simulation, which is caused by the division of the magnetic steel in Radia3D. The small ripples in the $\frac{\Delta B}{B}$ data are caused by the Hall probe accuracy being close to the difference in the field values between the measured points.

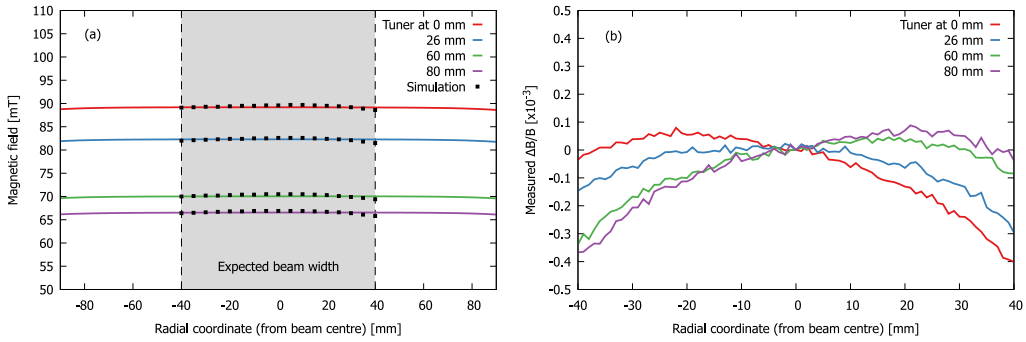

Fig. 9. (a) The measured and simulated magnetic field radially across the pole with different tuner positions. (b) The measured uniformity of the field, $\frac{\Delta B}{B}$ radially across the pole with different tuner positions.

5. Outlook

The first experiments with the CUBE-ECRIS have confirmed that the required beam currents translating to particle fluxes of 1–10 pnA can be achieved for argon charge states from 6+ to 10+, relevant for the IBA application. The achieved beam current and charge states are already higher than those achieved with other ECR ion sources with unconventional (simplified) B-field topologies, i.e. the 6.4 GHz ARC-ECRIS [10] with (electromagnet) minimum-B quadrupole structure and the 10 GHz PM ring ECRIS, PK-GANESA [11], producing charge states up to Ar^{6+} and Ar^{3+}, respectively.

There are apparent ways to improve the CUBE-ECRIS performance and reach not only higher intensities but higher charge states as well. These include using a slit extraction aperture (instead of the round aperture applied here), which matches the pattern of the escaping plasma flux. With the slit we are expecting a factor of five improvement in the beam currents of different charge states. Another method to improve the performance of the CUBE-ECRIS would be to increase the microwave power from 250 W as it is obvious from Fig. 3 that as it stands, the ion source performance is power-limited.

After experiments with the slit extraction in the present test stand setup we intend to change the electromagnet dipole to the prototype permanent magnet dipole. The permanent magnet dipole is expected to reduce beam transport losses as it has a wider pole gap of 90 mm vs. the electromagnet 70 mm pole gap. We plan to use the permanent magnet dipole to demonstrate the feasibility of the high charge state IBA-concept with argon and probe a possible extension to heavier elements (krypton and xenon). The permanent magnet ion source and m/q-separation allows minimising the power consumption of equipment on the 500 kV high voltage deck, which relaxes the technical requirements of the ancillary equipment, required to operate the platform, in comparison to conventional ECR ion source and electromagnetic separation of the ions.

Declaration of competing interest

The authors declare that they have no known competing financial interests or personal relationships that could have appeared to influence the work reported in this paper.

Acknowledgments

This work has been supported by the STFC Horizons Programme: investigating solutions for net zero and Academy of Finland Project funding N:o 315855.

References

[1] M. Döbeli, C. Kottler, F. Glaus, M. Suter, Nucl. Instrum. Methods Phys. Res. Section B: Beam Interact. Mater. Atoms 241 (1–4) (2005) 428–435.
[2] C. Kottler, M. Döbeli, F. Glaus, M. Suter, Nucl. Instrum. Methods Phys. Res. Section B: Beam Interact. Mater. Atoms 248 (1) (2006) 155–162.
[3] J. Julin, T. Sajavaara, Nucl. Instrum. Methods Phys. Res. Section B: Beam Interact. Mater. Atoms 406 (Part A) (2017) 61–65.
[4] T. Kalvas, O. Tarvainen, V. Toivanen, H. Koivisto, J. Instrum. 15 (2020) P06016.
[5] T. Kalvas, V. Toivanen, S.T. Kosonen, H. Koivisto, O. Tarvainen, L. Maunoury, Plasma Sources. Sci. Technol. 31 (2022) 12LT02.
[6] http://dx.doi.org/10.23729/042aa259-d34c-4cbc-8e02-e1b40be6e4df (Accessed 30 September 2022).
[7] P. Elleaume, O. Chubar, J. Chavanne, Proc. PAC97, Vancouver, Canada 12–16, 1997, pp. 3509–3511, http://www.esrf.eu/Accelerators/Groups/InsertionDevices/Software/Radia.
[8] A.R. Bainbridge, J.A. Clarke, Proc. IPAC2017, Copenhagen, Denmark, THPIK105, jacow.org.
[9] https://neorem.fi/wp-content/uploads/2019/04/hysteresis-graph-712a.pdf (Accessed 30 September 2022).
[10] P. Suominen, T. Ropponen, H. Koivisto, Nucl. Instrum. Meth. A. 578 (2007) 370.
[11] P. Salou, L. Maunoury, G. Gaubert, M. Michel, N. Lecesne, R. Leroy, D. Besnier, AIP Conf. Proc. 2011, 2018, p. 040021.